JOURNAL OF AIRCRAFT
Vol. 30, No. 4, July–Aug. 1993

Computation of Induced Drag for Elliptical and Crescent-Shaped Wings

Stephen C. Smith*
NASA Ames Research Center, Moffett Field, California 94035
and
Ilan M. Kroo†
Stanford University, Stanford, California 94305

Recent interest in the induced drag characteristics of crescent-shaped wings has led to a closer look at the methods used for determination of induced drag from computational aerodynamic methods. Induced drag may be computed by integration of surface pressure or by evaluation of a contour integral in the Trefftz plane. A high-order panel method was used to study the induced drag of elliptical and crescent-shaped wings using both techniques. Induced drag computations using surface pressure integration were strongly affected by panel density and angle of attack. Drag computations for the crescent wing were especially sensitive to spanwise panel density because of the complex flowfield near the tip. Trefftz-plane results for the two wing planforms were not sensitive to panel density or angle of attack. The effect of correctly modeling the force-free, rolled-up wake geometry on the predicted span efficiency was demonstrated for both wing planforms. The span efficiency predicted from Trefftz-plane integration was about 0.97 for the elliptical wing and 0.99 for the crescent wing, both somewhat less than the classical theoretical maximum for planar wings. Most of the apparent drag reduction of the crescent wing claimed in previous studies was probably an artifact of the surface-pressure integration. The slightly higher span efficiency for the crescent wing was attributed to a more nearly elliptical spanwise lift distribution.

Nomenclature

AR	=	wing aspect ratio, b^2/S
b	=	wing span
C_{Di}	=	induced drag coefficient
C_L	=	lift coefficient
D_i	=	induced drag, $C_{Di}\rho/2V_\infty^2 S$
da	=	differential area element
ds	=	differential length element
e	=	span efficiency, $C_L^2/C_{Di}\pi AR$
e_{SP}	=	span efficiency computed by surface-pressure integration
e_{TR}	=	span efficiency computed by Trefftz-plane integration
N_c	=	number of chordwise panels on each surface
N_s	=	number of spanwise panels
$\boldsymbol{n}$	=	unit normal vector
S	=	wing area
u, v, w	=	wind-axis velocity components
V	=	velocity
X_t	=	x coordinate of wingtip, referenced to the root chord[8]
x	=	chordwise body-axis components
y	=	spanwise axis coordinate
α	=	angle of attack
Γ	=	circulation
ρ	=	density
σ	=	source strength
ϕ	=	perturbation potential

Received March 19, 1990; presented as Paper 90-3063 at the AIAA 8th Applied Aerodynamics Conference, Portland, OR, Aug. 20–22, 1990; revision received May 20, 1992; accepted for publication May 23, 1992.

*Research Engineer, Advanced Aerodynamic Concepts Branch. Member AIAA.
†Associate Professor, Department of Aeronautics and Astronautics. Member AIAA.

Introduction

REDUCTION of cruise drag continues to be an area of active research because of the potential for fuel savings on commercial aircraft. Minimizing induced drag is an important aspect of wing design, since it represents nearly half of the cruise drag. Traditionally, classical lifting-line or Weissinger methods have been used to design wings with minimum induced drag.[1,2] These methods are adequate for modeling many important aspects of wing performance, including the interactions of nonplanar lifting elements such as winglets. More detailed studies of the effects of wing geometry and wake deformation on induced drag require panel methods that model the actual wing surface.[3,4] Induced drag is often determined from panel methods by integrating surface pressure data, although far-field "Trefftz-plane" analysis is considered more reliable.[5,6]

In the last decade, attention has been directed toward more subtle aspects of wing design and their influence on induced drag. Zimmer[7] suggested that wing tip shape has a significant effect on induced drag. Van Dam[8] raised the possibility that certain planar wing planforms with highly swept tips may have lower induced drag than the classical theoretical minimum. Van Dam used the low-order panel method, VSAERO,[3] to study various "crescent moon-shaped wings," shown in Fig. 1. The family of wings studied in Ref. 8 were defined by elliptical chord distributions and NACA 0012 airfoils, with the leading edge defined by ellipses of increasing eccentricity. The x coordinate of the tip (X_t) was defined by the leading-edge eccentricity. Induced drag was computed by integrating surface pressures on models with 1000 surface panels (N_c = 50, N_s = 10). The iterative wake relaxation feature of VSAERO was used to model the rolled-up trailing wake.

The relative induced drag of a wing may be expressed by the span efficiency factor e, defined as the ratio of the induced drag of an elliptically loaded wing to the induced drag of a particular wing of the same span and total lift. The span efficiency of these crescent wings as computed in Ref. 8 are shown in Fig. 2. Van Dam computed a span efficiency of 1.0

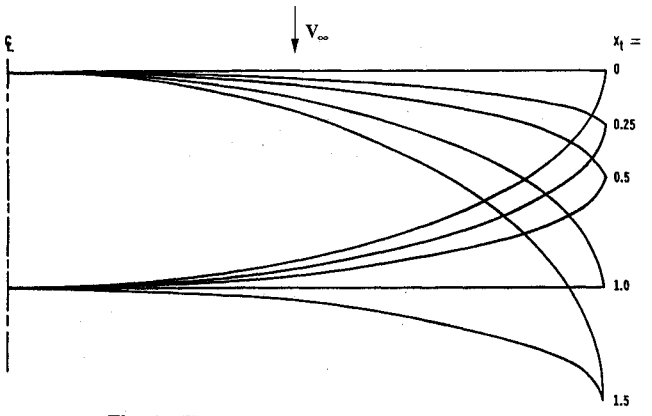

Fig. 1 Various crescent moon-shaped wings.[8]

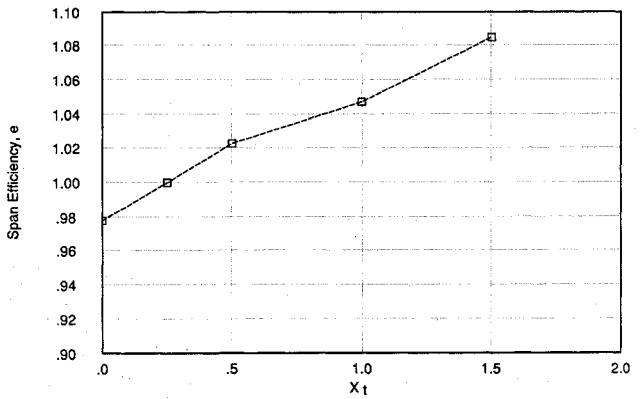

Fig. 2 Computed span efficiency for various crescent-shaped wings from Ref. 8.

for the elliptical wing with straight quarter-chord line (X_t = 0.25) and larger values of span efficiency as the wing tip was sheared back (up to 1.08 for X_t = 1.5). He hypothesized that the higher span efficiencies were related to favorable interactions of the rolled-up wake on the wing. Wind-tunnel investigations have also shown drag savings for these crescent wings, although the savings are of the same order as the experimental uncertainty.[9,10]

These results raise the somewhat surprising possibility of planar wings with lower induced drag than the elliptical wing. However, they also raise questions about the planform shape that best approximates the elliptical span loading, the influence of the rolled-up trailing wake, the numerical accuracy of induced drag computation by surface pressure integration, and the use of other techniques for determining induced drag from computational methods. The objective of the present study is to examine these problems of computational induced drag prediction as they apply to the induced drag of elliptical and crescent-shaped wings.

Methodology

A high-order panel method with very high resolution geometric modeling was used in an effort to achieve the highest possible accuracy. Induced drag was determined by integrating the surface-pressure distribution and from Trefftz-plane quantities. Elliptical and crescent-shaped wings were analyzed to evaluate the effects of panel density, wake modeling, and planform characteristics on induced drag.

Panel Method

The high-order panel method, A502 (PANAIR) applies a quadratic distribution of doublets and a linear distribution of sources over each panel with doublet and source matching at each panel edge.[4] This model is equivalent to a linearly varying distribution of vorticity over each panel. Indirect mass-flux boundary conditions are imposed by the setting the source strength to $\sigma = -V_\infty \cdot \boldsymbol{n}$, (known) and solving for the doublet strength (unknown) so that $\phi = 0$ on the interior. The Kutta condition is imposed by the explicit vorticity matching at the trailing edge, and the trailing wake is equivalent to a sheet of distributed vorticity. The A502 program includes a scheme for obtaining forces and moments by surface-pressure integration that is consistent with the linear vorticity distribution.

Wake Modeling

Linear solution of the panel method requires that the trailing wake geometry be prescribed. To study the effects of wake geometry on induced drag computation, both freestream and force-free wake models were used. For the paneling sensitivity evaluation, the trailing wake paneling was extended 36 semispans downstream of the wing in the freestream direction. It should be noted that this straight wake is not necessarily planar, but rather takes on the shape of the trailing edge projected onto the Trefftz plane. The crescent planform with straight trailing edge (X_t = 1.0) does have a planar wake, whereas, the classical elliptical wing (X_t = 0.25) has an elliptical wake trace in the Trefftz plane.

A force-free wake model was generated using a time-marching unsteady vortex-lattice method.[11] The resulting discrete vortex wake was used to define the geometry of the high-order wake panels for the A502 code. Although the wake generated by the vortex-lattice code looked qualitatively correct, Trefftz-plane analysis indicated that the wake shape was inaccurate. An alternative scheme was developed which used the high-order panel method to find the velocities induced on the wake from the wing, and the customary vortex method to find the velocities induced by the wake. This approach proved to be a robust method of creating accurately rolled-up free wake geometries.

Surface-Pressure Integration

It is well-known that numerical integration of surface pressure to compute drag is a very poorly conditioned problem. The aft-facing surfaces of the wing have a shallow slope, so that only a small component of the pressure acts in the freestream direction. The forward-facing surfaces have larger slopes, but the pressure distribution has large gradients in the vicinity of the leading edge, making it difficult to accurately resolve the large component of pressure in the streamwise direction. To further aggravate the problem, the contributions from the fore- and aft-facing surfaces largely cancel, leaving only a small value of drag which is vulnerable to numerical error. These errors may vary systematically with wing planform shape, since, e.g., local leading-edge sweep causes a reduction in attachment-line pressure and/or a more pronounced suction peak that may not be resolved as well.

There is some temptation to evaluate the pressure-integrated drag at zero angle of attack, where the inviscid drag is exactly zero, to form a "drag tare" to be used to adjust pressure-integrated drag results at other angles of attack. Although this may be effective in correcting for errors in integrating the thickness-dependent pressure distribution, it cannot correct for the error in resolving the pressure distribution due to angle of attack. The local surface slope and panel density at the location of the suction peak and the stagnation point change with angle of attack, so the "tare" is not representative of the pressure integration error, even at small angles of attack. No adjustment of surface-pressure integrated results were made in this study.

Trefftz-Plane Integration

The induced drag may also be found by the integration of pressure and momentum over a control volume surrounding the wing. When the control volume extends to infinity, only the surface integral over the exit plane remains:

$$D_i = \rho/2 \int\int (w^2 + v^2 - u^2)\, da$$

When the trailing vorticity is confined to a thin wake sheet and the u component is negligible, this integral reduces to a

contour integral along the intersection of the trailing vortex wake with the control-volume exit plane.[12] This so-called Trefftz-plane integral relates the induced drag to the jump in potential across the wake, and the "normal-wash" velocity through the wake:

$$D_i = \rho/2 \int (\phi_{\text{upper}} - \phi_{\text{lower}})(V \cdot \boldsymbol{n})\, ds$$

An approximation is introduced by the reduction to a contour integral when the wake is deflected from the freestream. This error is of order $(\varepsilon)^2$, where ε is the local angle between the wake vorticity and the freestream.[13]

Trefftz-plane surveys were made 18 semispans from the wing. To measure the trailing wake properties needed for Trefftz-plane integration, pairs of survey points were located along the wake a very small distance above and below the wake, shown in Fig. 3. The A502 program computed the velocity and perturbation potential at these points. The velocity in the wake at a particular station was then found by averaging the velocities of the corresponding survey points, and the jump in potential across the wake is found by the difference in potential between the two points.

Geometry

Induced drag was computed for two wing geometries corresponding to the $X_t = 0.25$ and the $X_t = 1.0$ geometries of Ref. 8. The $X_t = 0.25$ wing is a classical elliptical wing with a straight quarter-chord line, whereas, the $X_t = 1.0$ wing has an elliptical leading edge and a straight trailing edge. The $X_t = 1.0$ wing is particularly interesting because a trailing wake modeled straight off the trailing edge in the freestream direction is planar at all angles of attack. This planform will be referred to as a crescent wing, although it does not have the extreme sweep of the $X_t = 1.5$ planform. Both wings had an aspect ratio of 7.0, NACA 0012 airfoils, and no twist. As in Ref. 8, the wings were analyzed at an angle-of-attack of 4 deg, producing a lift coefficient of about 0.34, representative of cruise conditions.

The surface paneling in the chordwise direction was defined by a half-(cosine)$^{1.25}$ spacing from the leading edge to the maximum thickness point at 30% chord, and uniform spacing from 30% chord to the trailing edge with some additional panels added near the trailing edge. This distribution produced somewhat higher panel density near the leading edge than cosine spacing. The spanwise panel spacing was defined by a half-(cosine)$^{0.85}$ spacing, which concentrated more panels near the wing tip than a cosine distribution. These panel spacings seemed to provide the most satisfactory resolution of the pressure distribution over the wing. The wing tip was cropped at a span-fraction of 0.9995 and closed with additional panels. Figure 4 shows typical panel arrangements on the $X_t = 0.25$ elliptical wing a), and $X_t = 1.0$ crescent wing b), with 1000 panels ($N_c \times N_s = 50 \times 10$ on the upper and lower surfaces).

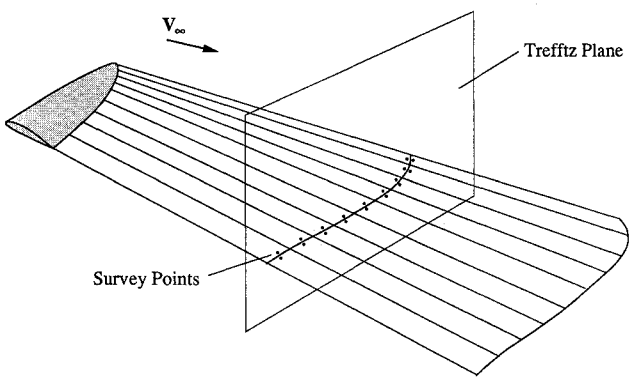

Fig. 3 Trefftz plane survey to compute induced drag.

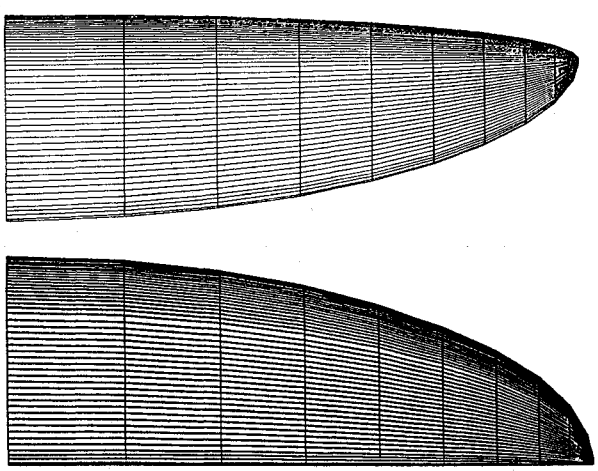

Fig. 4 Typical panel models of elliptical (above) and $X_t = 1.0$ crescent (below) wings, $N_c \times N_s = 50 \times 10$.

Results and Discussion

Sensitivity to Paneling

The sensitivity of induced drag calculated by surface-pressure integration to variations in surface panel density was investigated by analyzing both wing geometries with a range of panel densities. The span efficiency for each case was determined from the lift and drag coefficients computed by surface-pressure integration within the A502 code.

The variation of span efficiency for the crescent and elliptical wings with spanwise panel refinement is shown in Fig. 5. Initial studies focused on refining both the chordwise and spanwise paneling, but found that 70–80 chordwise panels on each surface were adequate. This is evident from the cases with panelings of $N_c \times N_s = 72 \times 36$ and 86×36 for the crescent wing, which have nearly the same computed span efficiency. Spanwise panel density had a strong effect on the pressure-integrated span efficiency, especially for the crescent wing. The span efficiency predicted for the crescent wing decreased almost 7% as N_s was increased from 10 to 69. For the same panel refinement, the elliptical wing span efficiency decreased almost 3%. As the spanwise panel density was increased, the predicted drag difference between the two planforms decreased from 6 to 1.8%. The computed span efficiency for both planforms continued to decrease, even with $N_s = 69$, over 11,000 total panels—requiring cpu time well beyond practical limits for most applications. The initial decrease in span efficiency is most likely associated with more accurate resolution of the three-dimensional flow near the wingtip. Errors in pressure integration are apparently planform-dependent when the spanwise resolution is inadequate. As the panel density is increased further, resolution of the surface pressures becomes less of a problem, but other numerical or discretization errors seem to make convergence of

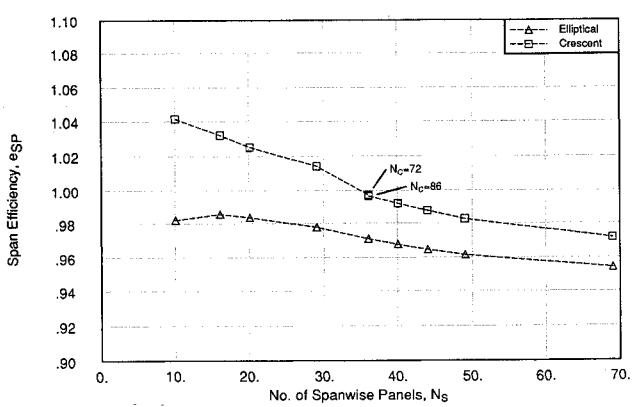

Fig. 5 Effect of spanwise panel density on span efficiency of elliptical and crescent wings, computed by surface-pressure integration.

the induced drag difficult. Reference 14 demonstrated very similar convergence properties with the Douglas panel method.

For each of these cases, the induced drag was also determined by Trefftz-plane integration, shown in Fig. 6. Span efficiency was computed from the Trefftz-plane drag and the pressure-integrated lift. There is some sensitivity of the Trefftz-plane results to spanwise panel spacing since the distribution of wake properties is integrated numerically. However, with $N_s = 10$, the computed drag of the elliptical wing was within 1% of the result with $N_s = 20$, and within 1.5% of the result with $N_s = 69$. The computed span efficiency of the crescent wing was 0.85% better than the elliptical wing—about half the drag reduction predicted from surface-pressure integration.

Sensitivity to Angle of Attack

To further study the sensitivity of the pressure integration, each wing geometry was run at various angles of attack. For the untwisted geometries studied here, the span efficiency should not vary with angle of attack, except for the (very small) effect of the nonplanar wake on the elliptical wing, which should increase span efficiency at higher angles of attack. As angle of attack is varied, the location and shape of the leading-edge suction peak changes, affecting the accuracy of the surface-pressure integration. In addition, the induced drag at low angles of attack is quite small, so numerical error may have a significant impact on the integration; at higher angles of attack, the induced drag is much greater and the impact would be lessened. The variation of span efficiency found by surface-pressure integration (shown in Fig. 7) seems to indicate that this is indeed the case. Even with very high panel density ($N_c \times N_s = 86 \times 36$), the pressure-integration results show strong dependence on angle of attack. No such dependence on angle of attack is evident in the Trefftz-plane integration, as shown in Fig. 8.

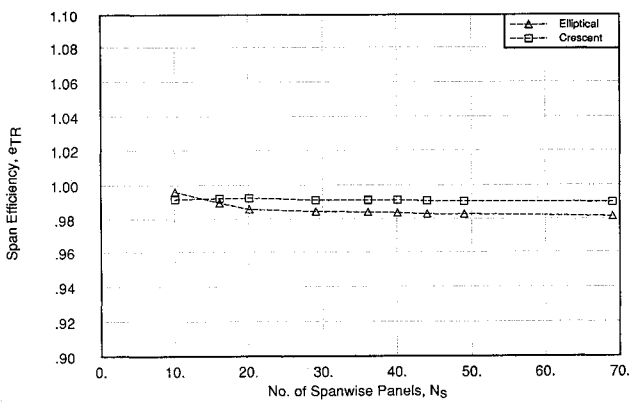

Fig. 6 Effect of spanwise panel density on span efficiency of elliptical and crescent wings, computed by Trefftz-plane integration.

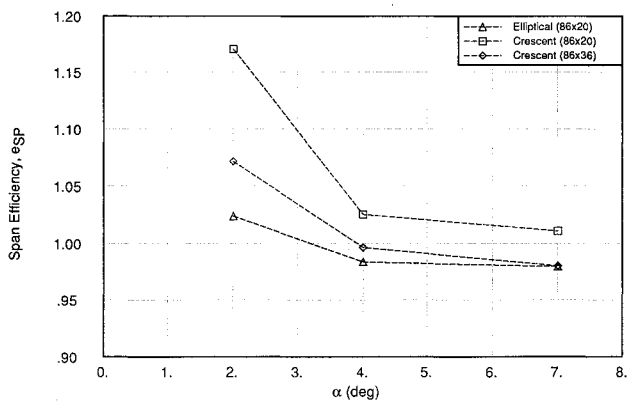

Fig. 7 Effect of angle of attack on span efficiency of elliptical and crescent wings, computed by surface-pressure integration.

Wake Modeling Effects

These results have shown that surface-pressure integration does not provide reliable drag predictions, even with impractically high panel density, whereas the Trefftz-plane analysis provides consistent results over a wide range of panel density and angle of attack. Since this study was done with the trailing wake modeled straight back in the freestream direction, a question may be raised about the effect of this approximation on the difference between the drag computed from the Trefftz plane and pressure integration. Although the straight wake is not force-free, it is drag-free, since the vorticity is parallel to the freestream. Therefore, the Trefftz-plane drag is expected to agree with the drag that would be determined from a perfect pressure integration, and any disagreement between the Trefftz plane and pressure integration must be an artifact of inaccurately computing or integrating the surface pressures. Whatever influence the replacement of the real force-free wake with a straight wake model has on the induced drag, it should be equally evident in the surface pressure distribution and the Trefftz plane.

The influence of the wake geometry on induced drag may be anticipated from the discussion in Ref. 13, where the classical momentum control volume is subdivided by a near-field plane as shown in Fig. 9. The portion of the force-free wake which lies between this near-field partition and the Trefftz plane may be replaced by a straight extension of the wake shape at the partition without changing the drag computed in the Trefftz plane. Of course the straight wake is only drag-free; the Trefftz-plane lift would be effected. For a wing with a straight, unswept trailing edge, this near-field plane may be moved very close to the trailing edge, and the entire rolled-up wake may be replaced by a straight wake without changing the computed drag. For the classical elliptic wing, a portion of the rolled-up wake remains when the partition is located

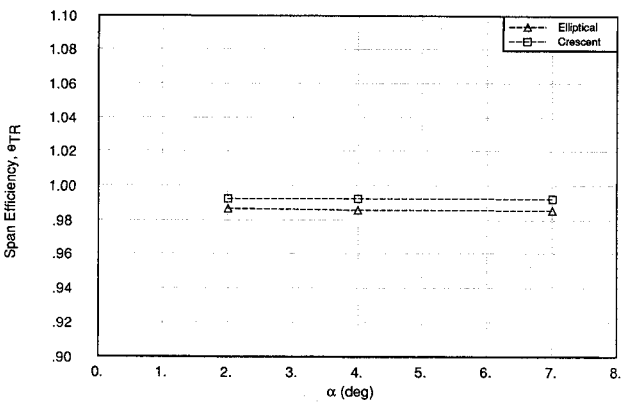

Fig. 8 Effect of angle of attack on span efficiency of elliptical and crescent wings, computed by Trefftz-plane integration.

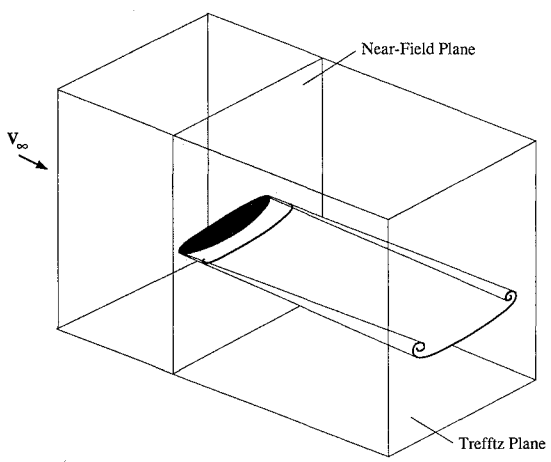

Fig. 9 Near-field plane subdividing control volume, from Ref. 13.

immediately downstream of the trailing edge at the root. Replacing this portion of the free wake with a straight wake is expected to introduce an error in the drag. To assess the magnitude of the drag error on the elliptical wing with straight wake, free wakes were generated for the crescent and elliptical planforms.

A force-free wake geometry with 50 trailing vortices was developed with the unsteady vortex-lattice method of Ref. 11 for the (X_t = 1.0) crescent wing. This wake geometry was modeled with 17 spanwise panels to match a $N_c \times N_s$ = 64 × 17 panel model of the wing. Induced drag was computed by both surface-pressure and Trefftz-plane integration for both wake geometries. These results are given in Table 1.

The free wake had some effect on the induced drag computed by surface-pressure integration; the computed span efficiency decreased by 1.8%, but because of the relatively course panel density used, these values are probably not meaningful. On the other hand, the Trefftz-plane drag changed rather dramatically, decreasing more than 8%. Although it is true that there are higher-order errors associated with the Trefftz integral when the wake is not parallel to the freestream,[13] this was not the problem here. Numerical integration of the momentum through the entire exit plane yielded similar results. The source of error was in the details of the wake shape. Recall that the Trefftz integration gives the induced drag within the control volume. An error in the wake shape implies that the wake is not drag free, and leads to an error in the computed drag. This wake-shape error arises from the basic nature of the vortex-lattice method used to relax the wake. The wake shape is determined by velocities computed from the bound and trailing vortex systems. But vortex-lattice and constant-doublet panel methods have velocity singularities at the panel edges, and the velocities are correct only at the control points. Significant velocity errors exist at other points in the field, particularly on the wake near the trailing edge.[15]

To solve this problem, a hybrid scheme was developed which uses the accurate velocities from the high-order panel method for the influence of the wing on the wake, and the customary vortex method for the wake-induced velocities. Although the wake appeared qualitatively correct after just three relaxation iterations, 12 iterations of this hybrid approach were used to generate a wake with sufficient geometrical accuracy to insure accurate Trefftz-plane drag computation. Force-free wakes were generated for both the crescent and elliptical planforms modeled with $N_c \times N_s$ = 86 × 29 panels at an angle-of-attack of α = 3.57 deg. A comparison of the wake shapes generated by the two methods is shown in Fig. 10, indicating that a relatively small error in wake shape has a significant impact on the drag computed in the Trefftz plane.

Table 2 gives the results for both wing planforms with both straight and force-free wakes.

The results of the panel sensitivity study indicate that even with the high panel density used for this study of wake effects, the span efficiency found from pressure integration is probably not reliable, although the increment in span efficiency between the straight-wake and free-wake results is comparable to the Trefftz-plane results. The Trefftz-plane results are consistent with the hypothesis stated above. When a straight freestream wake is modeled with the elliptical wing, the computed span efficiency is about 1.5% higher than with the correctly modeled force-free wake, reflecting the error introduced by ignoring the initial roll-up ahead of the control-volume partition. On the other hand, the span efficiency of the crescent wing increases less than 0.2% with the straight-wake approximation, consistent with the conclusion that all the roll-up may be eliminated without changing the computed drag for this configuration.

Other Nonplaner Wake Effects

Attention has recently been focused on the nonplanar wake which is formed by the projection of the trailing edge shape into the Trefftz plane.[13,16,17] For the traditional elliptical wing at 4-deg angle of attack, the effective nonplanar height is $h/2b$ = 0.02, and the expected drag reduction from the nonplanar wake is about 1%.[13] However, this effect is overshadowed by the nonideal span loading. The crescent wing (X_t = 1.0) has a planar wake at all angles of attack, and therefore, has none of the nonplanar benefit, but maintains a more nearly ideal span loading. This nonplanar wake effect becomes more pronounced at higher angles of attack, and would have more impact on improving climb rather than cruise performance of aircraft.

Table 1 Effect of force-free wake from vortex-lattice method on the span efficiency of the crescent wing (X_t = 1.0)

	C_L	e_{SP}	e_{TR}
Straight freestream wake	0.3444	1.0325	0.9924
Force-free wake (vortex-lattice)	0.3432	1.0141	1.0819

Table 2 Effect of wake geometry on the span efficiency of the elliptical (X_t = 0.25) and crescent wing (X_t = 1.0) at α = 3.57 deg

	C_L	e_{SP}	e_{TR}
Elliptical wing:			
Straight freestream wake	0.30356	0.9781	0.9847
Force-free wake	0.29965	0.9685	0.9691
Crescent wing:			
Straight freestream wake	0.30666	1.0143	0.9915
Force-free wake	0.30353	1.0128	0.9897

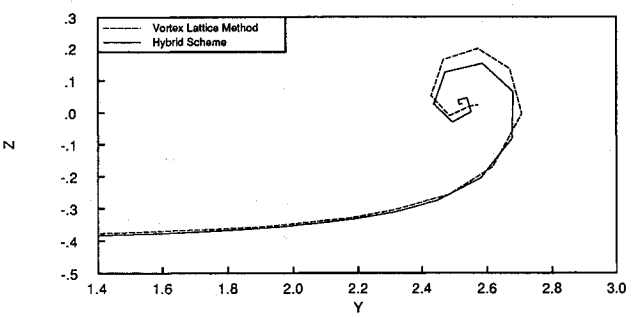

Fig. 10 Comparison of wake shape determined by vortex-lattice and hybrid methods; cross section 11.5 chords downstream of the crescent wing, $b/2$ = 2.75.

Comparison of Elliptical and Crescent-Shaped Wings

The spanwise distribution of lift and induced drag for the two wing planforms were determined by integrating the surface pressures on panel columns of constant span. The lift distributions for the crescent and elliptical wings at α = 4 deg, compared with a true elliptical loading, are shown in Fig. 11. The crescent wing (X_t = 1.0) exhibits a more nearly elliptical loading than the elliptical wing (X_t = 0.25). Recall that the classical elliptical wing concept arises from lifting line theory, where the trailing wake from an elliptical circulation distribution produces uniform downwash on an unswept lifting line. It follows that an elliptical chord distribution would produce the elliptical loading, since the induced angle of attack is constant. In reality, the downwash distribution over the actual wing surface where the bound vorticity is distributed is not uniform, leading to a somewhat nonelliptical loading. Of course, a truly elliptical circulation distribution is unachievable since it requires an infinite vorticity strength along the wake edge.

Figure 12 shows the distribution of induced drag along the span for both wing planforms. The induced drag distribution on the elliptical wing is nearly elliptical, reflecting more or less constant downwash along the span. The effects of sweep on the crescent wing modify the downwash distribution, and

therefore, the induced drag distribution along the span. Compared with the elliptical wing, the inboard portion of the crescent wing produces less lift and more drag, resulting from greater downwash. Similarly, induced upwash on the tip region creates a considerable amount of thrust. Spanwise panel density must be sufficient to resolve the strong spanwise pressure gradients indicated by this pattern in order to accurately determine the induced drag from surface pressure integration. This explains why the error in induced drag computation from insufficient spanwise panel density is so planform-dependent.

The variation of downwash along the wake trace in the Trefftz plane for the two geometries is shown in Fig. 13. Both wing planforms have some upwash near the tip resulting from the finite vorticity at the tip, although the downwash remains more nearly constant close to the wingtip on the crescent wing, consistent with the more nearly elliptical span loading. The downwash distributions of Fig. 13 also give some idea of why spanwise resolution near the tip is less important for Trefftz-plane integration; the jump in potential at the tip is rather small, and so this small region of nonuniform downwash contributes little to the value of the drag integral.

Figure 5 showed that the apparent drag savings between the crescent ($X_t = 1.0$) and elliptical planforms with straight-wake models changed from about 6 to 1.8% as the panel model was refined from $N_s = 10$ to $N_s = 69$. The 6% drag increment predcted with $N_s = 10$ is similar to the results of Ref. 8, allowing for the different wake model used. Figure 14 compares Trefftz-plane results from the present study and from Ref. 14 with the pressure-integration results of Ref. 8. Predicted span efficiency for elliptical and crescent planforms with both force-free and straight wake models are shown. These results suggest that much of the drag savings indicated in Ref. 8 are more likely an artifact of inaccurate pressure integration than a favorable interaction with the rolled-up wake. All of the planforms studied achieved span efficiencies slightly less than the classical maximum.

The 2% improvement in span efficiency shown here for the $X_t = 1.0$ wing is most likely due to the more nearly elliptical span loading. It is possible to modify the chord distribution of the $X_t = 0.25$ wing to achieve a more nearly elliptical span loading. The local chord of this wing was increased by the difference between the actual span loading and an ellipse at each spanwise panel edge. All the chords were then normalized so that the total wing area remained constant. This new planform was then reanalyzed to find the new span loading. Four iterations of this process led to the wing planform shown in Fig. 15. The spanwise lift distribution of this wing is as close to elliptical as the crescent wing, as shown in Fig. 16. The Trefftz-plane span efficiency of this wing modeled with a straight wake was 0.993, essentially the same as the crescent planform with the same panel density.

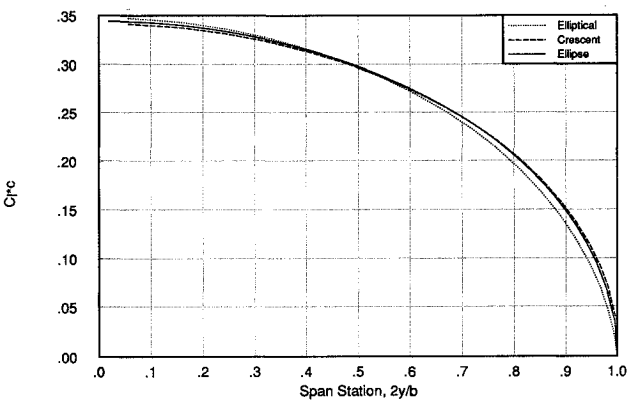

Fig. 11 Spanwise distribution of lift for the elliptical and crescent wings.

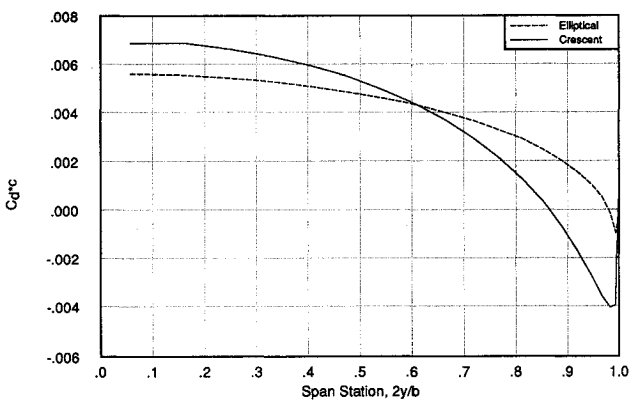

Fig. 12 Spanwise distribution of induced drag for the elliptical and crescent wings.

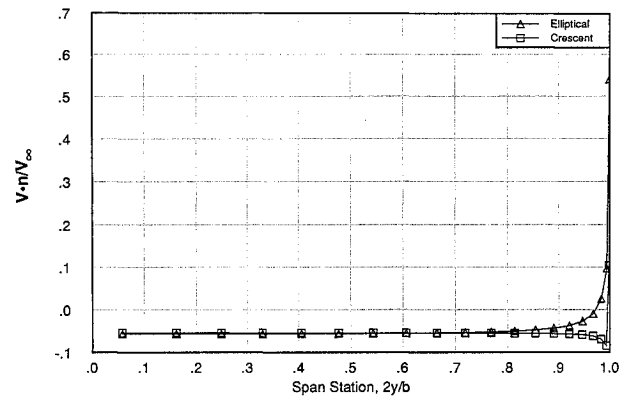

Fig. 13 Downwash distribution in the Trefftz plane for the elliptical and crescent wings.

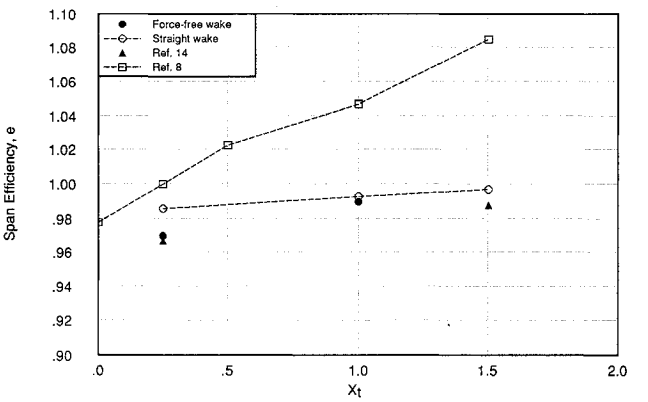

Fig. 14 Span efficiency computed in the Trefftz plane for various crescent-shaped wings, compared with pressure-integration results from Ref. 8.

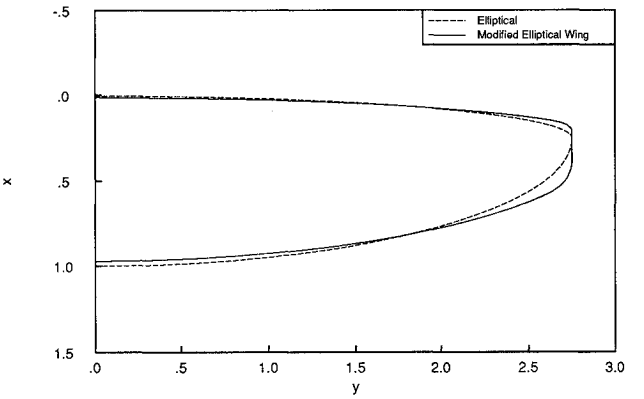

Fig. 15 Modified elliptical wing planform with elliptic spanwise lift distribution.

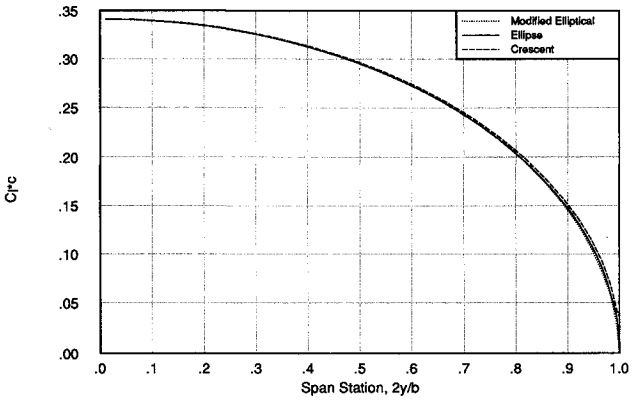

Fig. 16 Spanwise distribution of lift for the modified elliptical and crescent wings.

Conclusions

It is quite difficult to determine induced drag from computational methods with sufficient accuracy to assess the performance of the wing tip modifications. Whether the surface pressures are found from a Navier-Stokes code on a finite-difference grid or a surface-panel method, the resulting pressures must be integrated to find the induced drag. This integration is very sensitive to grid or panel density in both the chordwise and spanwise directions, and to numerical error. For methods which maintain a coherent trailing vortex wake, such as panel methods, the technique of Trefftz-plane integration may be used to determine induced drag without the high sensitivity to panel density or angle of attack.

Trefftz-plane analysis predicted a drag savings of about 0.85% for the crescent wing compared with the elliptical wing when both wings were modeled with straight wakes. This savings was attributed to a more nearly elliptical span loading. The span efficiency of both planforms was slightly less than 1.0. An elliptical wing modified to improve the span loading was shown to have the same span efficiency as the crescent planform. Substitution of a force-free, rolled-up wake geometry reduced the computed span efficiency of the crescent wing by only 0.18%, but reduced the predicted performance of the elliptical wing by about 1.5%. These results are consistent with a hypothesis based on an extension of the classical control-volume momentum theory. The computed span efficiencies of the elliptical and crescent wings, including accurately modeled free wakes, were 0.970 and 0.990, respectively. These results suggest that much of the apparent drag reduction of the crescent wing claimed in previous studies is probably an artifact of the pressure integration rather than an interaction with the nonplanar wake.

The Trefftz-plane integration of the rolled-up wake was found to be very sensitive to errors in the wake shape. The wake geometry generated from a vortex-lattice method was not sufficiently accurate, and a new scheme was developed which used induced velocity information from the high-order panel code as part of the wake relaxation. The new technique produced significantly more accurate wake shapes.

Wake roll-up effects must be accounted for if highly accurate drag comparisons are required, but the error in Trefftz-plane drag resulting from inaccurate wake shapes is potentially quite large. On the other hand, the error associated with the straight wake model is rather small and probably quite acceptable for routine performance estimation. This is fortunate, since the straight wake model is considerably less time consuming to generate than the correct force-free wake.

Other recent studies have indicated the potential for increased span efficiency when the trailing wake is not planar. In this study, the benefit of the nonplanar wake on the elliptical wing was probably outweighed by the less than ideal lift distribution. Nonplanar wake effects are expected to play a larger role at higher angles of attack, representative of climb rather than cruise conditions. Wingtip shapes which exaggerate these nonplanar wake effects while maintaining optimum span loading, may offer enough performance gain to warrant further research, and the results of this study provides a framework for accurately predicting their performance with computational techniques.

References

[1]Cone, C. D., Jr., "The Theory of Induced Lift and Minimum Induced Drag of Nonplanar Lifting Systems," NASA TR 139, Feb. 1962.

[2]Kroo, I. M., "A General Approach to Multiple Lifting Surface Design and Analysis," AIAA Paper 84-2507, Oct. 1984.

[3]Maskew, B., "Prediction of Subsonic Aerodynamic Characteristics—A Case for Low-Order Panel Methods," *Journal of Aircraft*, Vol. 19, No. 2, 1982, pp. 157–163.

[4]Carmichael, R. L., and Erickson, L. L., "PANAIR—A Higher Order Panel Method for Predicting Subsonic or Supersonic Linear Potential Flows About Arbitrary Configurations," AIAA Paper 81-1255, June 1981.

[5]Letcher, J. S., Jr., "Convergence of Lift and Drag Predictions by a Morino Panel Method (VSAERO)," *AIAA Journal*, Vol. 27, No. 8, 1989, pp. 1019, 1020.

[6]Towne, M. C., Strande, S. M., Erickson, L. L., Kroo, I. M., Enomoto, F. Y., Carmichael, R. L., and McPherson, K. F., "PAN AIR Modeling Studies," AIAA Paper 83-1830, July 1983.

[7]Zimmer, H., "The Aerodynamic Optimization of Wings in the Subsonic Speed Range and the Influence of the Design of the Wing Tips," Dr-Ing. Dissertation, Univ. of Stuttgart, Stuttgart, Germany, 1983.

[8]Van Dam, C. P., "Induced-Drag Characteristics of Crescent-Moon-Shaped Wings," *Journal of Aircraft*, Vol. 24, No. 2, 1987, pp. 115–119.

[9]Vijgen, P. M. H. W., Van Dam, C. P., and Holmes, B. J., "Sheared Wing-Tip Aerodynamics: Wind Tunnel and Computational Investigations of Induced-Drag Reduction," AIAA Paper 87-2481 CP, Aug. 1987.

[10]Van Dam, C. P., Vijgen, P. M. H. W., and Holmes, B. J., "Wind-Tunnel Investigation on the Effect of a Crescent Planform on Drag," AIAA Paper 90-0300, Jan. 1990.

[11]Mittelman, Z., "Prediction of Unsteady Aerodynamics and Control of Delta Wings with Tangential Leading Edge Blowing," Ph.D. Dissertation, Stanford Univ., SUDDAR-580, Stanford, CA, June 1989.

[12]Küchemann, D., *The Aerodynamic Design of Aircraft*, Pergamon, Oxford, England, UK, 1978, pp. 58–60.

[13]Kroo, I. M., and Smith, S. C., "Computation of Induced Drag with Nonplanar and Deformed Wakes," Society of Automotive Engineers Transactions, SAE Paper 901933, Long Beach, CA, Sept. 1990.

[14]DeHaan, M. A., "Induced Drag of Wings with Highly Swept and Tapered Wing Tips," AIAA Paper 90-3062-CP, Aug. 1990.

[15]Schlichting, H., and Truckenbrodt, E., *Aerodynamics of the Airplane*, McGraw-Hill, New York, 1979, p. 79.

[16]Burkett, C. W., "Reductions in Induced Drag by the Use of Aft Swept Wing Tips," *Aeronautical Journal*, Vol. 93, Dec. 1989, pp. 400–405.

[17]Lowson, M. V., "Minimum Induced Drag for Wings with Spanwise Camber," *Journal of Aircraft*, Vol. 27, No. 7, 1990, pp. 627–631.